J|A|C|S ARTICLES

Published on Web 07/22/2010

Local Current Mapping and Patterning of Reduced Graphene Oxide

Jeffrey M. Mativetsky,[†] Emanuele Treossi,[‡] Emanuele Orgiu,[†] Manuela Melucci,[‡,§] Giulio Paolo Veronese,[||] Paolo Samorì,[*,†] and Vincenzo Palermo[*,‡]

Nanochemistry Laboratory, ISIS - CNRS 7006, Université de Strasbourg, 8 allée Gaspard Monge, 67000 Strasbourg, France, Istituto per la Sintesi Organica e la Fotoreattività - Consiglio Nazionale delle Ricerche, via Gobetti 101, 40129 Bologna, Italy, Istituto di Chimica dei Composti Organometallici - Consiglio Nazionale delle Ricerche, via Madonna del Piano 10, 50019 Sesto F.no (Fi), Italy, and Istituto per la Microelettronica e i Microsistemi - Consiglio Nazionale delle Ricerche, via Gobetti 101, 40129 Bologna, Italy

Received May 26, 2010; E-mail: samori@unistra.fr; palermo@isof.cnr.it

Abstract: Conductive atomic force microscopy (C-AFM) has been used to correlate the detailed structural and electrical characteristics of graphene derived from graphene oxide. Uniform large currents were measured over areas exceeding tens of micrometers in few-layer films, supporting the use of graphene as a transparent electrode material. Moreover, defects such as electrical discontinuities were easily detected. Multilayer films were found to have a higher conductivity per layer than single layers. It is also shown that a local AFM-tip-induced electrochemical reduction process can be used to pattern conductive pathways on otherwise-insulating graphene oxide. Transistors with micrometer-scale tip-reduced graphene channels that featured ambipolar transport and an 8 order of magnitude increase in current density upon reduction were successfully fabricated.

Introduction

Graphene possesses unique electrical properties on account of its single-atom-thick two-dimensional honeycomb lattice structure.[1,2] Charge carriers act as massless Dirac fermions;[3] perturbations in the sheet lead to charge puddles,[4] and remarkable electron and hole mobilities result from the zero-gap semiconductor band structure.[3] Moreover, its high conductivity and optical transparency over visible wavelengths make graphene a candidate for large-area electrode applications such as solar cells and displays.[5−8] While rapid progress in measuring electrical transport in multilayer films and single graphene sheets has been achieved, little is known about the local spatial dependence of the electrical properties. Here we show that conductive atomic force microscopy (C-AFM)[9] is a powerful tool for obtaining direct measurements of the local variations in current-carrying capacity in graphene sheets and films over length scales ranging from tens of nanometers to tens of micrometers. These measurements make it possible to correlate the detailed morphology of graphene (e.g., wrinkles, multilayer regions) to its electrical characteristics. It is further demonstrated that a metallic AFM tip can be used to pattern electrically insulating graphene oxide (GO) with micrometer-scale conductive regions.

The conversion of GO to graphene through chemical reduction or thermal treatment is widely viewed as a promising pathway to mass production.[5,6,10−13] GO sheets consist of a graphitic carbon network bearing various types of oxygen-containing defects that render the sheets soluble in water. This allows the efficient processing and dispersion of isolated sheets or multilayer films from solution. Upon reduction of GO, a large portion of the oxygen-containing defects are removed, rendering the reduced GO (rGO) electrically conducting. The extent to which the graphitic network of sp^2 bonds is restored and the degree to which the properties approach those of pristine graphene are subjects of intense study.[10,13−17] Lattice defects

† Université de Strasbourg.
‡ Istituto per la Sintesi Organica e la Fotoreattività.
§ Istituto di Chimica dei Composti Organometallici.
|| Istituto per la Microelettronica e i Microsistemi.

(1) Geim, A. K.; Novoselov, K. S. *Nat. Mater.* **2007**, *6*, 183.
(2) Geim, A. K. *Science* **2009**, *324*, 1530.
(3) Novoselov, K. S.; Geim, A. K.; Morozov, S. V.; Jiang, D.; Katsnelson, M. I.; Grigorieva, I. V.; Dubonos, S. V.; Firsov, A. A. *Nature* **2005**, *438*, 197.
(4) Zhang, Y. B.; Brar, V. W.; Girit, C.; Zettl, A.; Crommie, M. F. *Nat. Phys.* **2009**, *5*, 722.
(5) Wang, X.; Zhi, L. J.; Müllen, K. *Nano Lett.* **2008**, *8*, 323.
(6) Becerril, H. A.; Mao, J.; Liu, Z.; Stoltenberg, R. M.; Bao, Z.; Chen, Y. *ACS Nano* **2008**, *2*, 463.
(7) Kim, K. S.; Zhao, Y.; Jang, H.; Lee, S. Y.; Kim, J. M.; Kim, K. S.; Ahn, J. H.; Kim, P.; Choi, J. Y.; Hong, B. H. *Nature* **2009**, *457*, 706.
(8) Pang, S. P.; Tsao, H. N.; Feng, X. L.; Müllen, K. *Adv. Mater.* **2009**, *21*, 3488.
(9) Mativetsky, J. M.; Palma, M.; Samorì, P. *Top. Curr. Chem.* **2008**, *285*, 157.
(10) Stankovich, S.; Dikin, D. A.; Piner, R. D.; Kohlhaas, K. A.; Kleinhammes, A.; Jia, Y.; Wu, Y.; Nguyen, S. T.; Ruoff, R. S. *Carbon* **2007**, *45*, 1558.
(11) Gilje, S.; Han, S.; Wang, M.; Wang, K. L.; Kaner, R. B. *Nano Lett.* **2007**, *7*, 3394.
(12) Eda, G.; Fanchini, G.; Chhowalla, M. *Nat. Nanotechnol.* **2008**, *3*, 270.
(13) Tung, V. C.; Allen, M. J.; Yang, Y.; Kaner, R. B. *Nat. Nanotechnol.* **2009**, *4*, 25.
(14) Gao, W.; Alemany, L. B.; Ci, L. J.; Ajayan, P. M. *Nat. Chem.* **2009**, *1*, 403.
(15) Jung, I.; Dikin, D. A.; Piner, R. D.; Ruoff, R. S. *Nano Lett.* **2008**, *8*, 4283.

10.1021/ja104567f **© 2010 American Chemical Society**

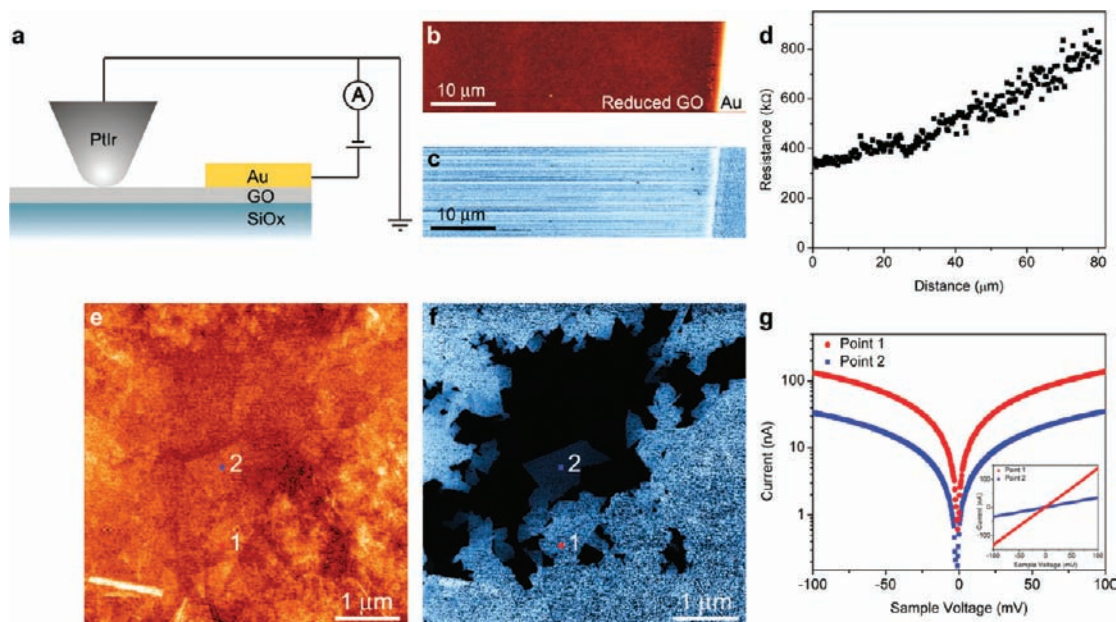

Figure 1. (a) Schematic of the setup employed for C-AFM current mapping and current–voltage acquisition. (b) Contact-mode topographic AFM image of a few-layer reduced GO (rGO) film with a top-contact Au electrode (z range = 115 nm) and (c) the simultaneously recorded current map obtained using a 100 mV sample voltage (current range = 200 nA). (d) Dependence of the electrical resistance on the separation between the tip and the counter electrode. Each data point represents an average of 20 measurements. (e) Contact-mode image of a defect region of an rGO film (z range = 6 nm) and (f) the corresponding current image, showing the absence of current over electrically disconnected segments and the differences in the current over regions of different thickness (current range = 200 nA). (g) Current–voltage traces measured at points 1 and 2 marked in (e) and (f). The inset shows the same data on a linear scale.

inevitably play an important role in the electrical transport, and therefore, techniques for elucidating the relationship between structure and electrical characteristics are needed. One technique that holds great potential for this type of study is C-AFM.[9] In this approach, a metal-coated AFM tip is used as a movable electrode that can be positioned with nanometer-scale precision and a controlled nanonewton-range force. In contrast to scanning tunneling microscopy (STM), the use of force feedback decouples the regulation of the tip–sample separation from the current measurement, providing a better-defined tip–sample interaction and the capability of measuring samples with insulating regions. Previous applications of C-AFM include studies of self-assembled monolayers,[18,19] organic semiconductors,[20] and low-dimensional nanostructures such as carbon nanotubes.[21] We demonstrate here that C-AFM is well-suited for mapping the local electronic properties of rGO.

There is also great interest in patterning graphene for large-scale integration into electronic devices and for prototyping lab-scale test systems. Large-scale patterned graphene films have been grown by chemical vapor deposition and transferred to flexible substrates.[7] Stencil masks have been used in conjunction with electrochemical[22] or camera-flash[23] reduction to produce macroscopically patterned rGO. Moreover, quantum confinement and opening of an energy band gap have been observed in graphene nanoribbons patterned by standard lithography methods.[24,25] However, it has been shown that lithography can leave residual photoresist on patterned graphene, potentially obscuring the intrinsic device characteristics.[26] We demonstrate a resistless single-step C-AFM-based approach for patterning GO with conductive micrometer-scale regions under ambient conditions. As a proof of principle, we have employed this technique to fabricate micropatterned graphene field-effect transistors featuring high charge-carrier mobilities.

Results and Discussion

Current Mapping of Reduced Graphene Oxide. GO was produced by a modified Hummers method as previously described[27] and then spin-coated onto Si substrates with a 300 nm thick SiO_2 layer. We first tested the applicability of C-AFM for current mapping on few-layer-thick thermally reduced rGO films obtained by annealing GO at 750 °C in an inert environment. This process is known to restore ~80% of the sp^2 network, yielding a conductive film, albeit with a lower conductivity than pristine graphene.[17]

C-AFM imaging was performed by applying a voltage between a Pt/Ir-coated AFM tip and a vacuum-deposited Au top electrode and scanning the tip over the sample with a constant force in the contact mode. A schematic of the setup is

(16) Gomez-Navarro, C.; Weitz, R. T.; Bittner, A. M.; Scolari, M.; Mews, A.; Burghard, M.; Kern, K. *Nano Lett.* **2007**, *7*, 3499.
(17) Mattevi, C.; Eda, G.; Agnoli, S.; Miller, S.; Mkhoyan, K. A.; Celik, O.; Mostrogiovanni, D.; Granozzi, G.; Garfunkel, E.; Chhowalla, M. *Adv. Funct. Mater.* **2009**, *19*, 2577.
(18) Wold, D. J.; Frisbie, C. D. *J. Am. Chem. Soc.* **2001**, *123*, 5549.
(19) Mativetsky, J. M.; Pace, G.; Elbing, M.; Rampi, M. A.; Mayor, M.; Samorì, P. *J. Am. Chem. Soc.* **2008**, *130*, 9192.
(20) Kelley, T. W.; Frisbie, C. D. *J. Phys. Chem. B* **2001**, *105*, 4538.
(21) Gomez-Navarro, C.; De Pablo, P. J.; Gomez-Herrero, J.; Biel, B.; Garcia-Vidal, F. J.; Rubio, A.; Flores, F. *Nat. Mater.* **2005**, *4*, 534.
(22) Zhou, M.; Wang, Y. L.; Zhai, Y. M.; Zhai, J. F.; Ren, W.; Wang, F. A.; Dong, S. J. *Chem.–Eur. J.* **2009**, *15*, 6116.
(23) Cote, L. J.; Cruz-Silva, R.; Huang, J. X. *J. Am. Chem. Soc.* **2009**, *131*, 11027.
(24) Berger, C.; Song, Z. M.; Li, X. B.; Wu, X. S.; Brown, N.; Naud, C.; Mayou, D.; Li, T. B.; Hass, J.; Marchenkov, A. N.; Conrad, E. H.; First, P. N.; de Heer, W. A. *Science* **2006**, *312*, 1191.
(25) Han, M. Y.; Ozyilmaz, B.; Zhang, Y. B.; Kim, P. *Phys. Rev. Lett.* **2007**, *98*, 206805.
(26) Ishigami, M.; Chen, J. H.; Cullen, W. G.; Fuhrer, M. S.; Williams, E. D. *Nano Lett.* **2007**, *7*, 1643.
(27) Treossi, E.; Melucci, M.; Liscio, A.; Gazzano, M.; Samorì, P.; Palermo, V. *J. Am. Chem. Soc.* **2009**, *131*, 15576.

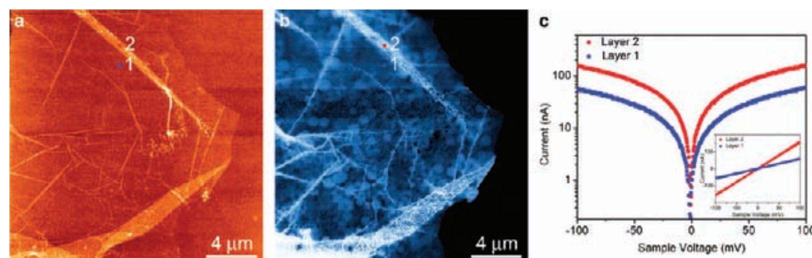

Figure 2. (a) Contact-mode topographic image of a single-layer rGO sheet exhibiting some folds and multilayer regions (z range = 6 nm). (b) Simultaneously recorded current map showing increased currents over the folded and multilayer regions as well as local variations over the single-layer areas (sample voltage = 100 mV, current range = 200 nA). The Au surface electrode is out of view, on the left side. (c) Current−voltage traces measured at points 1 and 2 marked in (a) and (b). The inset shows the same data on a linear scale.

shown in Figure 1a. The recorded current as a function of position provides a map of the local capacity of the sample to transport charge between the tip position and the Au counter electrode. As shown in Figure 1b,c, the current measured on a 3.7 ± 0.7 nm thick rGO film is highly uniform over a scale of tens of micrometers, highlighting the potential of rGO as a transparent electrode material.[5,6,8] Small line-to-line variations are visible, probably caused by microscopic structural changes in the tip−sample interface during scanning, particularly at the Au step edge. For this reason, and also to preserve the tip quality during the experiments, current imaging was often performed with the surface electrode outside the scan area. The bright appearance of the Au edge in the current image is related to the large topographic height difference at the edge (100 nm in this instance), which causes the side of the tip rather than the sharp apex to electrically contact the sample; this results in a larger contact area and an increased current. In addition, over the Au, the current map has a speckled appearance due to the formation and loss of contact with individual nanometer-scale Au grains by the tip as it scans over the surface. A relatively constant electrical contact between tip and sample was formed over the rGO as a result of its smooth morphology. Interestingly, there were no abrupt changes in conductivity associated with the rGO sheet edges, indicating efficient transport between adjacent sheets. This is in contrast to the case of organic semiconductors, where grain boundaries represent a major transport bottleneck.[20]

The resistance of the rGO film as a function of tip−electrode separation yielded a nearly linear relation (Figure 1d). Some nonlinearity is to be expected given the measurement geometry: the current spreads as it flows through the sample from the sharp tip to the extended Au electrode. Nonlinearities may also originate from the conduction mechanism. For example, in carbon nanotubes, as the concentration of divacancies is increased, the nonlinear transport becomes more pronounced as a result of coherent scattering at the defect sites.[21] Fitting the curve to a second-order polynomial yielded a contact resistance of 340 kΩ, representing the sum of the resistances at the rGO−electrode and rGO−tip interfaces. The latter is expected to be the dominant contribution, given the relatively small contact area of ~7 nm^2 (see the Supporting Information).

Topography and current images of a region with incomplete rGO coverage on SiO_2 (Figure 1e,f) show that defects in the rGO film are far more easily visualized in the current channel than in the topography. As displayed in Figure 1f, the electrical connectivity of the film and the local capacity to transport charge is immediately clear from the current image, while the topography (Figure 1e) provides little information with respect to these. The resolution of the current images was determined to be less than 20 nm on the basis of the minimum distance between distinct features. Current−voltage ($I-V$) measurements (90 in total) at 16 positions on the surface (Figure 1g) revealed currents over single-layer regions that were 3.9 ± 0.5 times smaller than the currents over multilayer regions at similar electrode distances. The film thickness of 3.7 ± 0.7 nm, which was measured over several areas of the sample, indicates that the film consisted of about three rGO layers, given the measured single-layer thickness of 1.2 ± 0.1 nm, the latter closely matching that of earlier studies.[6,16,27,28] By considering as an approximation the stacked rGO layers as parallel conductors, we see that the current per layer in the multilayer is 1.3 times larger than the current in the single layer. A similar effect was measured by Kern and co-workers,[16] who suggested that decreased conduction in the first layer results from interactions with the substrate. An additional factor may be that in multilayer graphene, there is an increased number of percolation pathways around defects. Moreover, in few-layer rGO films, the band structure is expected to depend on the number of layers. In the case of pristine graphene, as the number of layers increases, the band structure becomes increasingly semimetallic (i.e., there is increased band overlap).[29]

Further support for increased conductivity in multilayers was provided by C-AFM measurements on single rGO sheets. A topographic AFM image is shown in Figure 2 along with the corresponding current image. These measurements revealed a smooth single-layer morphology with narrow folds and two-layer segments; moreover, the current image shows that folded and two-layer regions are more conductive than the single-layer rGO, provided that the regions are in direct contact with the surface electrode. In instances where folded and multilayer regions are surrounded by single-layer rGO, the current is limited by the intervening single layer. $I-V$ measurements (44 curves at 22 points) showed that the current over the directly contacted two-layer regions was 3.0 ± 0.4 times larger than the current over the single layer. Assuming equal conduction in each layer, the current per layer in the bilayer was thus 1.5 times the current in the single layer. Two representative $I-V$ curves are shown in Figure 2c. Upon close inspection of the current image (Figure 2b), some round features and small local variations in current are visible over the single-layer regions, which may be due to the thermal reduction process (e.g., outgassing of the oxygen-containing defects). The resistance as a function of distance from the Au electrode was measured on a single-layer flake, and a nearly linear relation was obtained, similar to the multilayer case (see the Supporting Information).

(28) Jung, I.; Vaupel, M.; Pelton, M.; Piner, R.; Dikin, D. A.; Stankovich, S.; An, J.; Ruoff, R. S. *J. Phys. Chem. C* **2008**, *112*, 8499.
(29) Partoens, B.; Peeters, F. M. *Phys. Rev. B* **2006**, *74*, 075404.

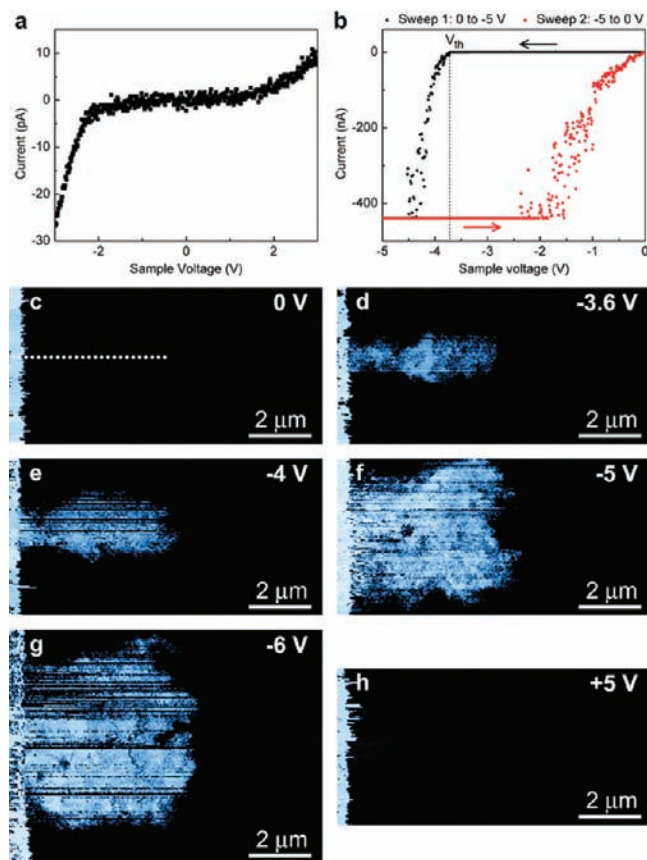

Figure 3. AFM-tip-induced modification of GO leading to conductive regions. (a) Current−voltage measurement on a few-layer GO film. (b) As the current was swept to large negative voltages, beyond a threshold voltage $V_{th} = -3.6 \pm 0.3$ V, the current suddenly increased to saturation levels of the current detection. Upon reversal of the sweep direction back toward zero, the currents remained high over most of the voltage range before returning to zero current at zero sample voltage. (c) Current map over GO contacted by a Au top electrode (at the left) showing currents over the Au but no measurable current over the GO at an applied bias of 100 mV. (d−g) Sweeping the sample voltage between zero and large negative voltages [(d) −3.6 V, (e) −4 V, (f) −5 V, (g) −6 V; voltage sweep rate = 1.2 Hz] at points spaced 500 nm apart along the trajectory shown in (c) produced conducting paths of varying width. (h) Positive sample voltages did not result in similar GO modification. The sample voltage during image acquisition was 100 mV, and the current scale is 12 nA in all of the images.

The extracted contact resistance of 1.1 MΩ is slightly more than 3 times higher than that in the multilayer.

Tip-Induced Reduction of Graphene Oxide. Not surprisingly, GO multilayers (7 ± 1 nm thick) without reduction exhibited limited electrical transport. At 2 μm from the Au electrode, picoampere-range currents were measured at voltages above 2 V (Figure 3a). Interestingly, a change took place when the tip was in close proximity to the Au electrode (e.g., within 1 μm) at negative sample voltages beyond −3.6 ± 0.3 V: the current rapidly increased with voltage from current levels below the minimum detection limit (<1 pA) to beyond the maximum detection limit (>500 nA), spanning more than 5 orders of magnitude. This change was marked by hysteresis in the $I-V$ traces (Figure 3b). Subsequent C-AFM imaging revealed that the GO surface was rendered conducting over a small patch of the surface. Sweeping the sample voltage to a large negative voltage (below −3.6 ± 0.3 V) at evenly spaced intervals (e.g., 500 nm) starting from the electrode allowed conducting lines to be patterned on the GO (Figure 3c−g). The width of the features depended linearly on the magnitude of the applied voltage within the measured range (see the Supporting Information), with lines as narrow as 1 μm at voltages of −3.6 V and features as wide as 6 μm at −6 V. As shown in Figure 3h, no significant increase in conductivity was observed at positive sample biases.

Similar results were obtained on multilayer and single-layer GO. To ensure that the observed conductivity was not related to damage to the underlying oxide, the tip-induced modification was reproduced on quartz substrates (see the Supporting Information). There was no significant change in the GO surface topography following surface modification, as confirmed by AFM height measurements, demonstrating that the process is nondestructive. Conversely, differences between treated and untreated areas were observed in AFM friction images, suggesting a change in the chemical nature of the surface[30] (see the Supporting Information).

The surface modification experiments were performed at relative humidity (RH) levels between 40 and 60%. In order to test the possible role of an adsorbed water layer during the tip-induced modification of GO, the RH level in the AFM chamber was gradually reduced using flowing argon. As the RH decreased, the surface modification became less pronounced (see the Supporting Information), and the widths of the features were reduced to submicrometer dimensions. Below ∼25% RH, surface modification was no longer observed. This suggests that water has a significant role in the surface modification process. It is well-known that in air, a several-monolayer-thick water layer readily adsorbs on hydrophilic surfaces. Moreover, when the AFM tip is in contact with the sample, a water meniscus forms around the tip and acts as a localized electrochemical environment. Previous studies have shown that through the application of a positive voltage between the tip and sample, it is possible to locally oxidize various substrates, including silicon[31] and graphene.[32] In the case of our experiments, it is expected that the GO was electrochemically reduced by the negative tip−sample voltage. Previous work on macroscopic electrochemical GO reduction revealed that reduction is facilitated at low pH levels, indicating an essential role of hydrogen ions.[22] It is likely that during the tip-induced modification, the water layer at the tip−GO interface is oxidized, thereby generating hydrogen ions that take part in reducing the GO. The required presence of water also rules out an alternative explanation, namely, thermal reduction of GO caused by resistive Joule heating, as such a mechanism would require temperatures[17] that would vaporize any adsorbed water and thus show an increase rather than a decrease in efficiency with decreasing RH.

Repeated tip-induced modification of the same GO region resulted in increased conductivity (Figure 4). After 10 modification cycles, the measured currents in the $I-V$ traces were 10 times higher than after the first modification and within an order of magnitude of the results for thermally reduced GO. The dependence of the current on the cycle number followed a sigmoidal growth trend (Figure 4b). Similar growth kinetics were observed for tip-induced silicon oxidation, where the transport of ions through the growing oxide barrier limits growth over time.[31] In the case of GO, it is expected that the decrease in

(30) Wilbur, J. L.; Biebuyck, H. A.; Macdonald, J. C.; Whitesides, G. M. *Langmuir* **1995**, *11*, 825.
(31) Avouris, P.; Hertel, T.; Martel, R. *Appl. Phys. Lett.* **1997**, *71*, 285.
(32) Weng, L. S.; Zhang, L. Y.; Chen, Y. P.; Rokhinson, L. P. *Appl. Phys. Lett.* **2008**, *93*, 093107.

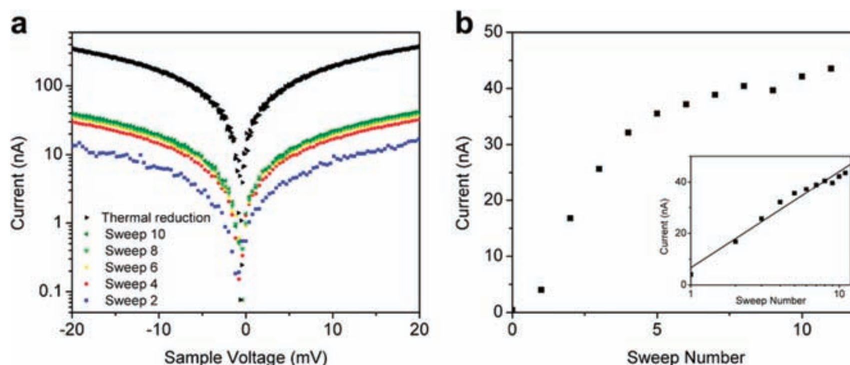

Figure 4. Repeated tip-induced modification of the same GO region results in increased conductivity. (a) Current−voltage traces recorded after multiple sample voltage sweeps to −5 V, showing an increase in current with increasing number of sweeps. After 10 voltage sweeps, the currents were within an order of magnitude of those for thermally reduced GO measured at the same tip−electrode distance of 2 μm. (b) The current measured at 20 mV increased with voltage sweep number according to a sigmoidal growth trend. The inset shows a nearly linear dependence on a linear−log plot.

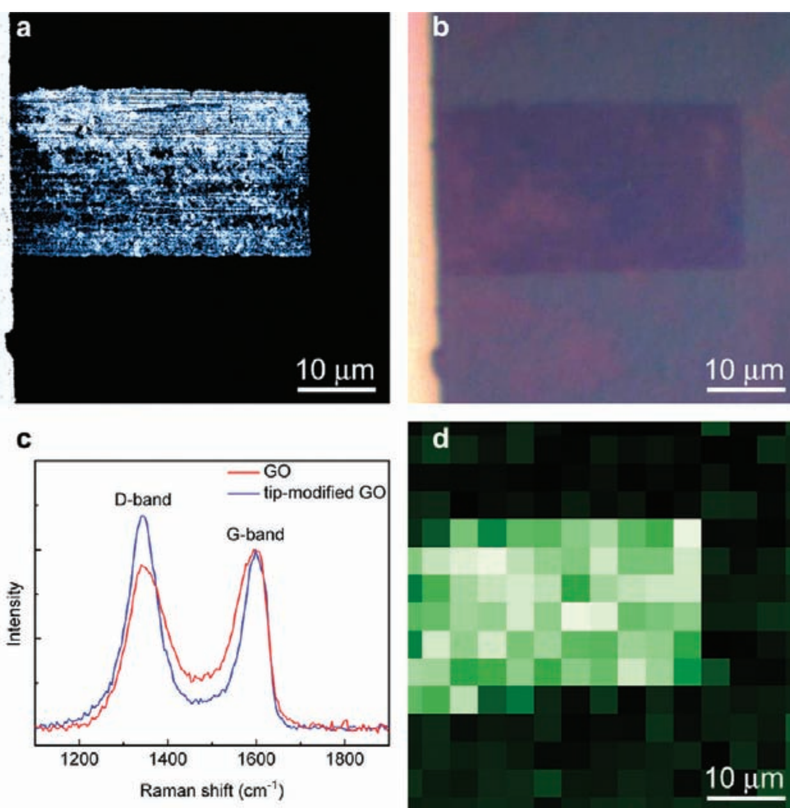

Figure 5. (a) C-AFM current map of a tip-modified rectangular region of a few-layer GO film and a top-contact gold electrode (left side; current range = 50 nA). (b) Optical image of the same region showing contrast between the modified and unmodified GO. (c) Raman spectra obtained on modified and unmodified GO (normalized to the G-band peak). (d) Raman map representing the spatial dependence of the D-band/G-band intensity ratio.

reduction rate with time is related to the depleted supply of oxygen-containing defects available to undergo reduction over time. A contact resistance of 1.3 MΩ was extracted for a GO region that was modified 11 times. With the assumption that the current was transported along the entire modified area, which had a width of 3.7 μm, a sheet resistance of 1 MΩ/square was determined; this is lower than the sheet resistance of 4 MΩ/square for hydrazine-reduced few-layer GO[11] but more than an order of magnitude higher than that for thermally reduced few-layer GO.[6]

Further evidence that the tip-induced GO modification corresponds to a reduction process was provided by confocal Raman spectroscopy, which is a particularly effective tool for identifying the structure and degree of disorder in carbon-based materials.[33,34] Large conductive GO features were patterned and subsequently measured by C-AFM, optical microscopy, and Raman spectroscopy (Figure 5). In accordance with previous studies,[6] the reduced region had a lower optical transmittance, resulting in a darker appearance under the optical microscope (Figure 5b). Raman spectra for the GO and modified GO exhibited two prominent peaks, at about 1350 and 1600 cm^{-1}, corresponding to the D and G bands. The G band is due to the E_{2g} phonon mode in the sp^2 carbon network, while the D band is correlated to disorder in the lattice.[34] In agreement with other

(33) Ferrari, A. C. *Solid State Commun.* **2007**, *143*, 47.
(34) Pimenta, M. A.; Dresselhaus, G.; Dresselhaus, M. S.; Cancado, L. G.; Jorio, A.; Saito, R. *Phys. Chem. Chem. Phys.* **2007**, *9*, 1276.

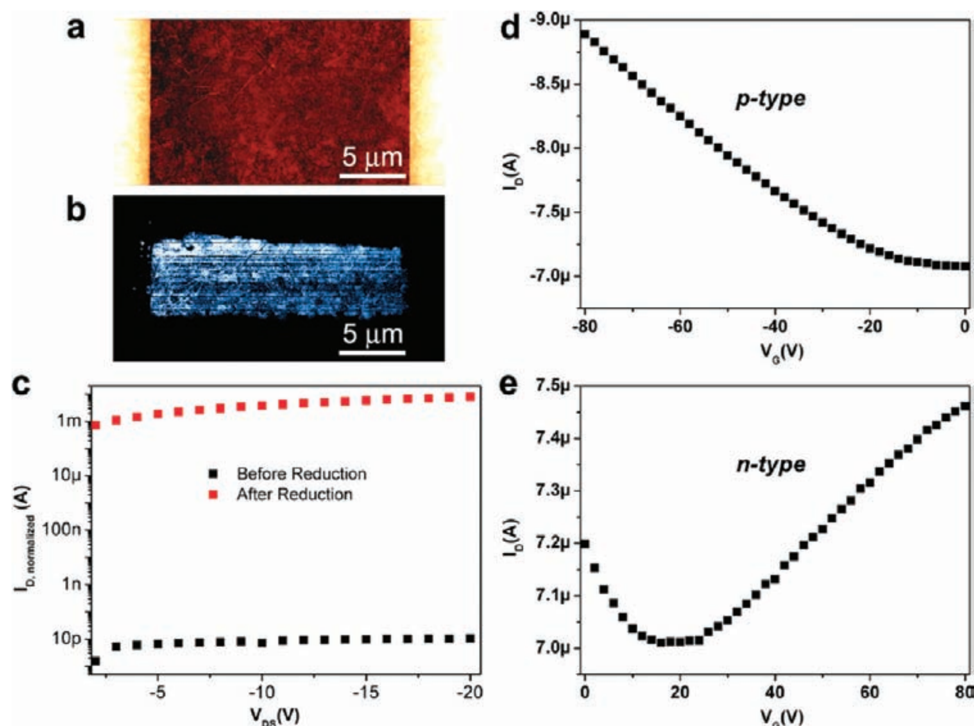

Figure 6. Thin-film transistors based on tip-reduced GO. (a) Topographic AFM image (*z* range = 60 nm) and (b) current image of a source−drain electrode pair (left and right side) bridged by an electrically conducting tip-reduced GO region (current range = 40 nA). Currents were not registered over the electrodes because the Au was covered by a film of unreduced GO. (c) Drain current (I_D) normalized to the effective channel width vs drain−source voltage (V_{DS}) measured on graphite oxide films before (black ■) and after (red ■) tip reduction. Prior to reduction, the channel width corresponds to the actual width of the electrode pairs, whereas following reduction, the channel width corresponds to the width of the reduced area (gate−source voltage $V_{GS} = -40$ V, channel length = 20 μm in both cases). An increase of $\sim 10^8$ in the normalized source−drain current is shown. (d, e) Transfer curves measured on the same tip-reduced GO transistor in the (d) p-type ($V_{DS} = -20$ V) and (e) n-type ($V_{DS} = +20$ V) transport regime.

studies,[10,13,22] the intensity of the D band increased relative to the G band upon reduction. This has been interpreted as resulting from the creation of new graphitic domains that are smaller in size but greater in number than those present prior to reduction.[10] The Raman map in Figure 5d, reconstructed from 15 × 15 (225) spectra, represents the spatial dependence of the D/G intensity ratio. The map of the tip-modified region corresponds well with the C-AFM and optical data, all of which support the interpretation that the tip-induced modification corresponds to localized reduction of GO.

Thin-Film Transistors Based on Tip-Reduced Graphene Oxide. The tip-induced reduction of GO was used to successfully bridge prepatterned top- or bottom-contact electrode pairs. Figure 6a,b shows a bottom-gate bottom-contact rGO transistor fabricated using this procedure. A channel width of 6 μm was defined with the AFM tip and then characterized by C-AFM, which revealed an estimated sheet resistance of 1.6 MΩ/square. Transistor measurements on several GO and tip-reduced GO devices in a nitrogen environment showed a significant current increase, approaching a factor of 10^8, obtained by means of tip reduction (Figure 6c). Mobility values were extracted from transfer curves in the linear regime (Figure 6c,d). The transport can be consistently considered ambipolar, as previously observed for reduced GO;[12] a hole mobility of 0.3 $cm^2\ V^{-1}\ s^{-1}$ and an electron mobility of up to 0.1 $cm^2\ V^{-1}\ s^{-1}$ were determined. These values are comparable to the ones measured by Chhowalla and co-workers,[12] who found p- and n-type mobilities of 1 and 0.2 $cm^2\ V^{-1}\ s^{-1}$, respectively, providing further evidence that the performance of the micropatterned AFM-tip-reduced GO is similar to that of GO reduced by combined hydrazine and thermal treatments. No degradation of the mobility was observed in the devices following 5 months of storage under nitrogen.

Conclusions

C-AFM was used to quantitatively assess the local electrical characteristics of reduced graphene oxide in different structural configurations (single layer, defects, multilayers) with a spatial resolution less than 20 nm. Exciting prospects exist for applying this approach to all types of graphene-based systems to correlate local morphological and electrical properties that are inaccessible to measurements that average over large areas. Moreover, the use of a metallic AFM tip for the local electrochemical conversion of GO to rGO having a tunable conductance and micrometer-scale feature size opens up paths to the rapid prototyping and testing of graphene devices with a single tool. As a proof of concept, micropatterned AFM-tip-reduced GO transistors were produced and shown to conduct 10^8 times more than unreduced GO transistors. Through parallel-tip[35] and stamp-based[36] approaches, there is also the potential to scale up local GO conversion for patterning graphene circuits over large areas.

During the review stage, it came to our attention that a very recent publication has reported on tip-induced reduction of GO based on a thermal process.[37]

Experimental Methods

SPM Characterization. AFM and C-AFM measurements were performed under ambient conditions, unless otherwise noted, using

(35) Minne, S. C.; Adams, J. D.; Yaralioglu, G.; Manalis, S. R.; Atalar, A.; Quate, C. F. *Appl. Phys. Lett.* **1998**, *73*, 1742.
(36) Losilla, N. S.; Martinez, J.; Garcia, R. *Nanotechnology* **2009**, *20*, 475304.

a Digital Instruments Dimension 3100 instrument equipped with a Nanoscope IV controller. Contact-mode Pt/Ir-coated silicon cantilevers (Nanosensors PPP-CONTPt) were employed for current mapping and local GO reduction. Standard dynamic-mode cantilevers (Veeco MPP-11120) were used for tapping-mode (intermittent-contact) imaging. During C-AFM measurements, a force of 15 nN was maintained; the tip was electrically grounded, and a bias voltage was applied to the sample. Tip velocities of 4−10 μm/s were used for C-AFM imaging, while $I-V$ measurements were recorded at a voltage sweep rate of 1.2 Hz. Unless otherwise noted, tip-induced GO reduction was performed by applying a −5 V pulse to the sample for a duration of 25 ms at sequential positions spaced 500 nm apart.

Raman Spectroscopy. Raman spectra were recorded on a Horiba Jobin Yvon Labram confocal Raman system with 532 nm laser excitation using minimal incident power in order to avoid heating effects.

Transistor Measurements. Electrical characterization was performed in an inert environment (glovebox) under a N_2 atmosphere using a Cascade Microtech M150 probe station. A Keithley 2636A SourceMeter interfaced with LabTracer 2.0 software was used to source voltages and collect data. Si/SiO_2 substrates with prepatterned electrodes were purchased from the Fraunhofer Institute for Photonic Microsystems. The substrates consisted of a highly doped Si gate ($n \approx 3 \times 10^{17}$ cm^{-3}), a 230 nm layer of thermally grown SiO_2 as a dielectric, and interdigitated electrodes having a 10 and 20 μm channel length, a 10 mm channel width, and a 40 nm height (30 nm Au on a 10 nm indium tin oxide adhesion layer).

Acknowledgment. We thank Simon Gree (Institut de Sciences des Materiaux de Mulhouse) for providing access to the Raman spectrometer and for his assistance with the Raman measurements. This work was supported by the ESF-EuroGraphene Project GOSPEL, the EC through the Marie-Curie RTN THREADMILL (MRTN-CT-2006-036040) and ITN-SUPERIOR (PITN-GA-2009-238177) as well as the EC FP7 ONE-P Large-Scale Project (212311), the NanoSciEra-SENSORS Project, and the International Center for Frontier Research in Chemistry (FRC, Strasbourg).

Supporting Information Available: Further details about the film thickness determination, C-AFM contact area, C-AFM measurements, and tip-induced GO reduction. This material is available free of charge via the Internet at http://pubs.acs.org.

JA104567F

(37) Wei, Z. Q.; Wang, D. B.; Kim, S.; Kim, S. Y.; Hu, Y. K.; Yakes, M. K.; Laracuente, A. R.; Dai, Z. T.; Marder, S. R.; Berger, C.; King, W. P.; de Heer, W. A.; Sheehan, P. E.; Riedo, E. *Science* **2010**, *328*, 1373.